

# PIV data: Vortex Detection and Characterization

Manuela Coletta<sup>1</sup>, Fabrizio De Gregorio<sup>2\*</sup>, Antonio Visingardi<sup>3</sup>, Gaetano Iuso<sup>1</sup>

<sup>1</sup>Politecnico di Torino, Mechanical and Aerospace Engineering Dep., Torino, Italy

<sup>2</sup>Italian Aerospace Research Centre, Aerodynamic and Icing Measurement lab., Capua, Italy

<sup>3</sup>Italian Aerospace Research Centre, Fluid Mechanics lab., Capua, Italy

\*f.degregorio@cira.it

## Abstract

The aim of the article is to propose a simple engineering method for identifying and characterizing vortical structures within a flow field measured with a classic two-component PIV measurement system. Some of the most popular vortex-detection systems are briefly presented. Of these, many fail if spurious vectors are present within the flow field due to poor PIV image quality. The investigated method is robust and reliable. The method is tested on synthetic images of ideal vortices and on real PIV images of a four-bladed rotor wake. The synthetic images have different spatial resolution and different noise level in order to perform a parametric assessment. Other vortex-identification schemes are applied for comparison.

## 1 Introduction

Many engineering applications deal with flows characterized by vortices. In particular, in the aeronautical field, the study of the aerodynamic characteristics of new fixed wing or rotary wing vehicles requires the identification and characterization of such structures.

The concept of vortex is intuitively a well-known flow phenomenon, present in many natural events and well investigated in fluid mechanics but a universally accepted definition of vortex is still missing. A first possible definition of vortex was given by Lugt (1983): "a vortex is the rotating motion of a multitude of material particles around a common centre". About ten years later, Robinson (1991) states that "a vortex exists when the instantaneous flow lines in the normal plane to the nucleus of the vortex, placed a moving observer together with the centre of the nucleus itself, exhibit a roughly circular or spiral movement". Although the definition of vortex is very ambiguous, over the years several criteria have been developed for the identification of vortices as discussed by Chakraborty et al (2005) and Kolar (2007). The most widely used local methods for vortex identification are based on the analysis of the velocity-gradient tensor  $\nabla u$ , its symmetric and antisymmetric parts, strain rate tensor  $\mathbf{S}$  and vorticity tensor  $\mathbf{\Omega}$ , respectively, and the three invariants of  $\nabla u$ . The paper presents the main vortex identification methods based on the velocity gradient tensor as: the Q criterion (Hunt et al 1988); the  $\Delta$  criterion introduced by Dallmann (1983), Vollmers et al. (1983), and Chong et al.(1990); the maximum of the velocity rotor and on the maximum of the circulation (Vollmers, 2001). These local vortex-detection criteria are not always suitable for PIV data affected by noise and spurious vector resulting in high velocity gradients. A possible solution was offered by the  $\Gamma_2$  criterion proposed by Graftieaux et al. (2001) and successfully applied to complex dynamic stall measurements on highly separated flow by Mulleners and Raffel (2011). The paper briefly illustrates in Section 2 some of the most popular vortex detection criteria together with the investigated one. Some synthetic images of theoretical vortices and some real PIV images of experimental test campaign have been used as test cases and are described in Section 3. The synthetic images were generated with different spatial resolutions, sizes, and noise levels in order to perform a parametric study. The real images include two characteristic cases: the presence of a body within the measurement field of view and a

highly turbulent flow. The obtained results are fully discussed in Section 4 and the main conclusions are drawn and illustrated in Section 5.

## 2 Vortex-identification schemes

### 2.1 Q-criterion

Hunt et al. (1988) identify vortices of an incompressible flow as connected fluid regions with a positive second invariant of  $\nabla\mathbf{u}$

$$Q = -\frac{1}{2}(u_x^2 + v_y^2 + w_z^2 + 2u_yv_x + 2u_zw_x + 2v_zw_y) = \frac{1}{2}(\|\bar{\Omega}\|^2 - \|\bar{S}\|^2) > 0 \quad (1)$$

that is, as the regions where the vorticity magnitude prevails over the strain-rate magnitude. In addition, the pressure in the vortex region is required to be lower than the ambient pressure.

### 2.2 $\Delta$ -criterion

Dallmann (1983), Vollmers et al. (1983), and Chong et al. (1990) define vortices as the regions in which the eigenvalues of  $\nabla\mathbf{u}$  are complex (a pair of complex-conjugate eigenvalues occurs) and the streamline pattern is spiralling or closed in a local reference frame moving with the point. Such points can be viewed within the critical-point theory – on a plane spanned by the complex eigenvectors – as elliptic ones (focus or centre). For incompressible flows, this requirement reads:

$$\Delta = \left(\frac{1}{2} R\right)^2 + \left(\frac{1}{3} Q\right)^3 > 0 \quad (2)$$

where Q and R are the invariants of  $\nabla\mathbf{u}$ , Q is given by eq. (1),  $R = \det(\nabla\vec{u})$ . Q and R play a key role in the reduced (due to incompressibility) characteristic equation for the eigenvalues  $\lambda$  of  $\nabla\mathbf{u}$ :

$$\lambda^3 + Q\lambda - R = 0 \quad (3)$$

### 2.3 Maximum vorticity criterion

The vorticity  $\vec{\omega} = \nabla \times \vec{u}$  reaches a local maximum in the centre of the vortex, so this feature can be exploited to identify the centre of the vortex (Vollmers 2001). Although this criterion can be very misleading, its vorticity is often measured as a first approximation to evaluate the intensity of a vortex.

### 2.4 Maximum of circulation criterion

The circulation  $\gamma$  reaches a local maximum in the centre of the vortex, so this feature can be exploited to identify the centre of the vortex. The circulation has been calculated following the method suggested by Vollmers (2001).

### 2.5 $\Gamma_2$ -criterion

The most widely used local methods for vortex identification are based on the analysis of the velocity-gradient tensor and its three invariants. In some cases, these local vortex-detection criteria are not suitable for PIV data, as for example in the regions affected by blade passages or the lower part of the rotor downwash where the tip vortex spirals are concentrated and the flow is highly turbulent. The possible solution is offered by the  $\Gamma_2$  criteria proposed by Michard and Favelier (2004). The function  $\Gamma_2$  is defined in discrete form as:

$$\Gamma_2(\vec{x}_i) = \frac{1}{M} \sum_{x_j \in S_i} \frac{\{(\vec{x}_j - \vec{x}_i) \times (\vec{u}_j - \vec{u}_{mean})\} \cdot \vec{n}}{|\vec{x}_j - \vec{x}_i| |\vec{u}_j - \vec{u}_{mean}|} \quad (4)$$

with  $S_i$  a two-dimensional circle around  $x_i$  with radius D, M the number of grid points  $x_j$  inside  $S_i$  with  $j \neq i$ ,  $\vec{n}$  the unit normal vector and  $u_j$  the velocity at  $x_j$ . According to its definition,  $\Gamma_2$  is a 3D dimensionless scalar function, with  $-1 \leq \Gamma_2 \leq 1$ . The zones delimited by  $|\Gamma_2| > \frac{2}{\pi}$  identify the vortices depicted by the measurement region. The vortex centre is identified as the maximum of the absolute

value of  $\Gamma_2$  in the delimited zone. For each identified vortex, the centre position is measured and the main characteristics, in terms of swirl velocity, vorticity and circulation are calculated along the vortex radius. The choice of the domain radius  $D$  have an influence on the dimension of the identified vortices and on the accuracy of the centre detection. In order to assess the reliability of the criteria a parametric investigation is performed using a single or a pair of vortices.

### 3 Test Cases

#### 3.1 Synthetic Vortex

In order to assess the reliability of the  $\Gamma_2$  criteria, a parametric investigation was carried out by using numerically-generated velocity fields containing a single (main) or a couple (main plus secondary) of theoretical vortices, co-rotating or counter rotating. In particular, the Vatistas (1998) vortex core model was used for the purpose, according to which the swirl velocity is expressed as:

$$V_{\theta} = \frac{\Gamma}{2\pi} \left[ \frac{r}{(r^{2n} + r_c^{2n})^{\frac{1}{n}}} \right] \quad (5)$$

This model was normalized with respect to  $\frac{|\Gamma_1|}{2\pi}$ , being  $|\Gamma_1|$  the module of the circulation of the main vortex, and its core radius  $r_{c1}$ , thus yielding the expression:

$$\bar{V}_{\theta} = \frac{\Gamma}{|\Gamma_1| r_{c1}} \left[ \frac{\bar{r}}{(\bar{r}^{2n} + \rho^{2n})^{\frac{1}{n}}} \right] \quad (6)$$

where  $\bar{r} = r/r_{c1}$ ,  $\rho = r_c/r_{c1}$  and the coefficient  $n$  was set equal to “1.06” as suggested by Scully (1975).

The capability of the criteria to detect vortices, even in the presence of white noise backgrounds, and to take into account the influence of a secondary vortex in the flow field, was tested by generating several velocity fields on a squared XY Cartesian grid. The computations were performed by varying: the spatial resolution of the grid ( $\Delta L/r_c = 0.5, 0.2, 0.1$  and  $0.05$ ); the vortex strength  $\frac{\Gamma}{|\Gamma_1|} = [\mp 0.5; \mp 1; \mp 2]$ ; the distance of the secondary vortex with respect to the main one; the amplitude of the white noise background, expressed as a percentage of the maximum value of the swirl velocity of an isolated vortex of unit strength ( $V_{\theta, max} \sim 0.52$ ). At the same time, the local vortex-identification criteria based on the velocity gradient were applied for comparison.

#### 3.2 Four-bladed rotor set-up

A dedicated rotor test rig was developed in the framework of the GARTEUR AG22 activities (Visingardi et al 2017) based on an existing commercial radio-controlled helicopter model (Blade 450 3D RTF), but largely customized and modified for the scope of the experiment, Figure 1. A four-bladed rotor with collective and cyclic control replaced the original two-bladed rotor hub. The rotor presented four untwisted, rectangular blades with radius of  $R=0.36$  m, root cut-out at 16% of the radius, chord length of  $c=0.0327$ m and a NACA0013 airfoil throughout the blade span, Figure 1. The resulting rotor solidity value was equal to  $\sigma=0.116$ . The clockwise rotor maximum speed was  $\Omega=1780$  rpm, and the collective pitch angle  $\theta_0$  varied from 1 to 11.3 degree.

The rotor downwash characteristics were measured by a standard two components measurement system composed by a double head Nd-Yag laser with a maximum energy of 320 mJ per pulse at 532 nm and a single double frame CCD camera (2048 by 2048 px). In order to track the blade tip vortices in the proximity to the rotor disk, measurement were performed using a 200 mm focal length obtaining a field of view of about 120 x 120 mm<sup>2</sup> and an optical resolution was about 17 px/mm. The time delay between the laser double-pulses was 25  $\mu$ s. The results presented a velocity spatial resolution of  $\Delta x=0.93$  mm. The random noise of the PIV cross-correlation procedure can be estimated as 0.1 px as a rule-of-thumb. Using the current values for the optical resolution (17 px/mm) and the laser double-pulse delay (25  $\mu$ s), this related to a velocity error of  $\Delta V$  of  $\sim 0.23$  m/s for the tip vortex measurements.

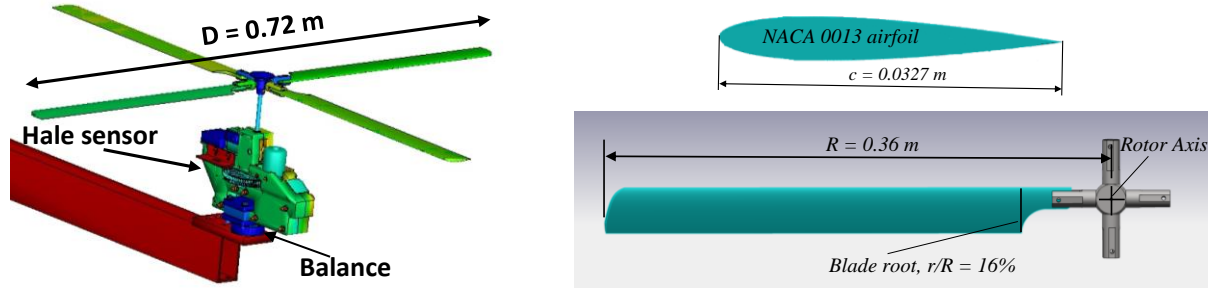


Figure 1: Rotor test rig (left image) and airfoil and planform blade drawings (right image).

The measured blade tip vortex core radius (defined as the distance from the vortex centre to the radial position where the maximum tangential velocity is reached) was between 3mm to 3.3mm so the ratio  $\Delta x / r_c$  was of about 0.31-0.28 comparable with the limit value of  $\Delta x / r_c \leq 0.2$  indicated by Martin et al. (2000) in order to assure a correct vortex characterization. In particular the vortex identification criteria are tested in proximity of the rotor blade where the tip vortex are well defined but the blade can lay in the field of view inducing strong reflection and at about one radius downstream the rotor disc where strong instability is present and the velocity fluctuation increases.

## 4 Results

The main results obtained on the synthetic and real velocity fields are fully discussed in the following.

### 4.1 Synthetic image

The single normalized Vorticity is centred in the origin of the Cartesian axis, has core radius equal to 1 and the velocity field size is 20 by 20 times the core radius. The parametric study foresaw the investigation of the single vortex for different spatial resolutions ( $\Delta L / r_c = 0.5, 0.2, 0.1, 0.05$ ) and with different white noise levels (0%, 20%, 70%, 90%). The  $\Gamma_2$  criteria is applied varying the domain radius  $D$  in the range from 2 to 15 in order to find a relationship between the domain radius and the image spatial resolution. The main characteristics of the synthetic single vortex are summarised in Table 1 for different spatial resolution.

Table 1: Synthetic Vortex main characteristics

$\Delta L / r_c$	0.5	0.2	0.1	0.05
$r_c$	1	1	1	1
$\Gamma$	$2\pi$	$2\pi$	$2\pi$	$2\pi$
Matrix size	40x40	100x100	200x200	400x400
N. of samples in $r_c$	2	5	10	20

Figure 2 shows that the  $\Gamma_2$  criterion accurately detects the correct centre of the synthetic single vortex without noise for any spatial resolution and any selected radius  $D$ . It is worth noting that the smallest domain radius ( $D=2$ ) provides the most accurate results. Once the centre of the vortex has been identified, the swirl velocity trend is plotted as the spatial resolution varies together with the theoretical Vorticity curve. The obtained maximum swirl velocity data indicate a negligible error with respect to the theoretical curve except for the case with spatial resolution  $\Delta L / r_c = 0.5$ , where the error is about the 4% of the maximum speed being the spatial resolution larger than the limit of  $\Delta L / r_c = 0.2$  indicated by Martin (2000). Similarly, the other vortex-detection criteria also correctly identify the centre of the vortices and the characteristics.

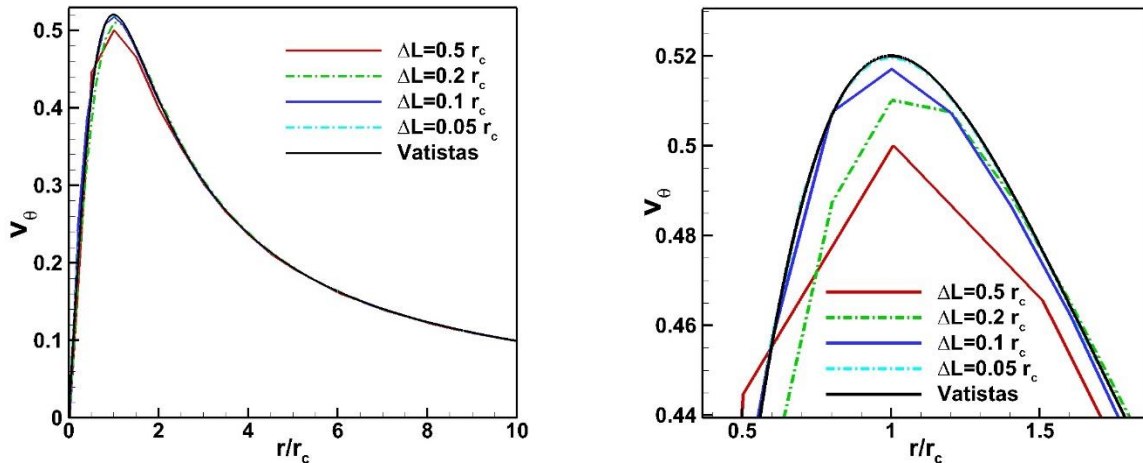


Figure 2: Swirl Velocity vs normalized radius for different spatial resolutions.

The analysis of the synthetic images with different levels of noise provides information on the relationship between the vortex core spatial resolution and the correct value of the  $\Gamma_2$  radius to be set. The measurement error of the vortex centre is defined as

$\varepsilon(V_c)\% = \frac{\sqrt{\Delta x_c^2 + \Delta y_c^2}}{\sqrt{\Delta x^2 + \Delta y^2}}\%$  where  $\Delta x_c$  and  $\Delta y_c$  are the axial components of the detected centre distance to the theoretical centre and  $\Delta x$  and  $\Delta y$  are the components of the spatial resolution. In the current case,

being the velocity matrix equi-spaced, the formula becomes  $\varepsilon(V_c) = \frac{\sqrt{\Delta x_c^2 + \Delta y_c^2}}{\Delta L \sqrt{2}}\%$ . Error smaller than the 50% indicates that the detected centre falls inside the same cell grid of the theoretical vortex.

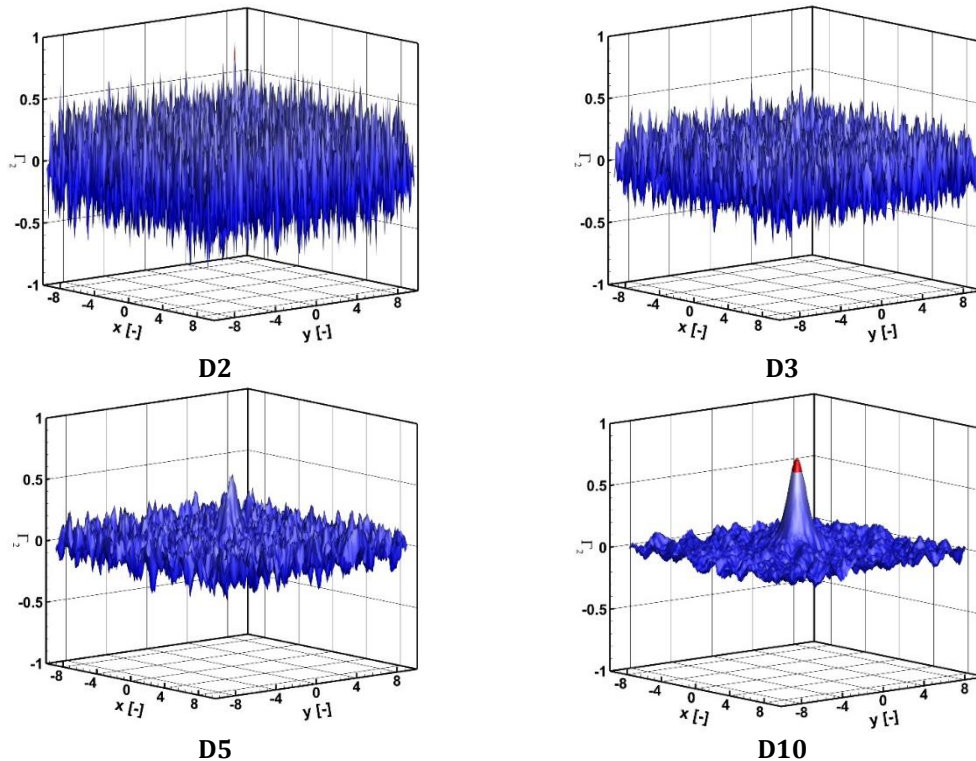


Figure 3:  $\Gamma_2$  functions for different radii of synthetic vortex with  $\Delta L/r_c=0.1$  and noise: 90%.

The  $\Gamma_2$ -criterion results indicate that increasing the noise level of the synthetic images, the smaller value of the radius fails in detecting the vortex centre. The  $\Gamma_2$  function for small radius values becomes too sensible to the noise presenting several erroneous peaks or does not reach the threshold value (Figure 3). The best result is obtained setting the domain radius equal to the number of sample points present along the core radius. Table 2 summarises the error values of the  $\Gamma_2$  criteria for a fixed spatial resolution of  $\Delta L/r_c=0.1$  and varying the domain radii and noise levels. For each noise level the minimum error is reached by  $D=10$ , further increasing the domain radius the error slightly increase.

Table 2: Vortex centre error  $\varepsilon(V_c)\%$  for spatial resolution of  $\Delta L/r_c=0.1$  for different noise levels.

$D$	2	3	5	10	15	25
Noise: 0%	0.1%	0.1%	0.1%	0.1%	0.1%	0.2%
Noise: 20%	34.9%	2.9%	0.8%	0.5%	0.5%	11.1%
Noise: 70%	\	\	36.1%	1.5%	2.4%	8.7%
Noise: 90%	\	\	\	35.1%	46.9%	36.6%

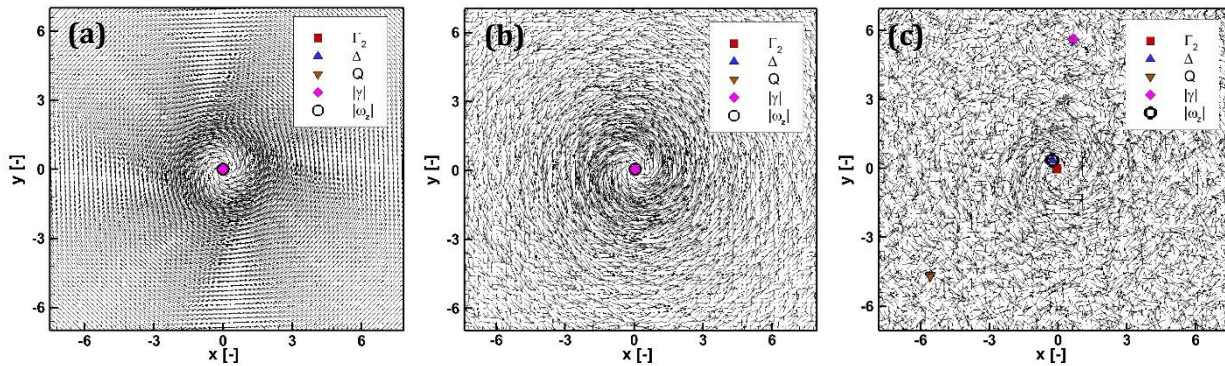


Figure 4: Vatisas Vortex - Velocity field and detected centres with different criteria. Noise 0% (a), noise 20% (b) and noise 90% (c)

The  $\Gamma_2$  criterion has better results in identifying the centre of the vortex than the other selected methods as the noise level increases. Without noise or for a 20% of noise all criteria correctly identify the centre (Figure 4 a and b). For noise of 70%, the  $\Delta$  and  $Q$  criteria detect the centre three mesh cells far from the correct position whereas the circulation  $\gamma$ -criterion is completely mistaken. For the case with noise of 90%, the  $\Delta$  and  $\omega_z$  criteria miss the identification of the vortex of about four mesh cells whereas the  $Q$  and  $\gamma$  criteria completely fail to detect the correct centre, as shown in Figure 4 c. Table 3 summarises the centre location error.

Table 3: Vortex detection error comparison varying the noise level.

Criterion	$\Gamma_2$	$\Delta$	$Q$	$\omega_z$	$\gamma$
Noise: 20%	0.5%	43.8%	17.9	51.7%	10.6%
Noise: 70%	1.5%	181.2%	181.2%	49.0%	7385.0%
Noise: 90%	35.1%	305.7%	5145.5%	305.7%	4003.3%

For the sake of completeness, Figure 5 shows the functions obtained by the different vortex identification criteria for different noise levels in order to give a clear picture of the criteria sensitivity to the noise. Once that the centre is located (red circle in Figure 5), the main vortex characteristics are calculated by the velocity matrix.

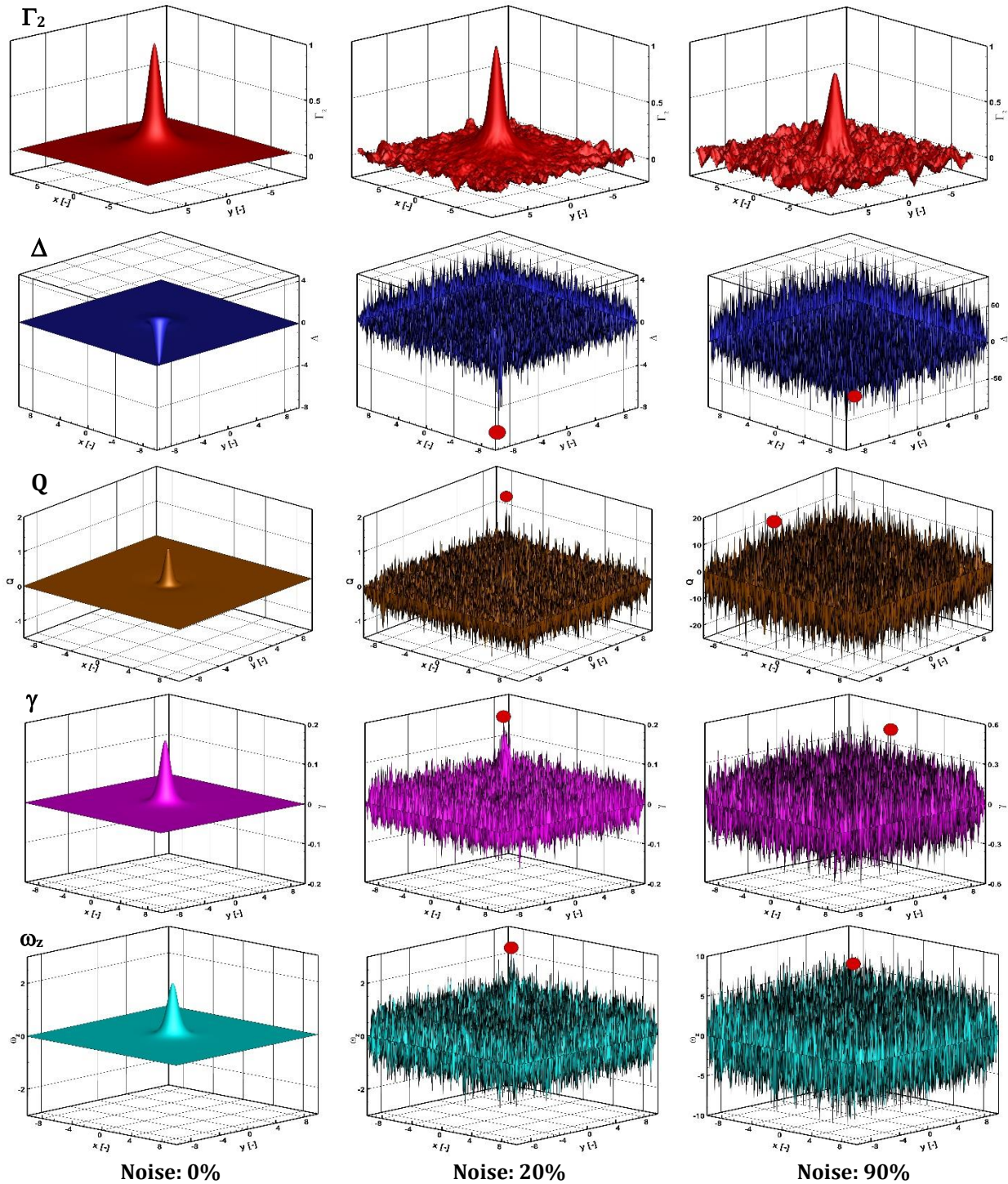


Figure 5: Vortex detection criteria applied to Vavtistas vortex for different noise levels.

In particular, Figure 6 shows the swirl velocity calculated by all the criteria for noise of 0%, 20% and 90%, respectively. Figure 6 c shows the consequence of the wrong centre location.

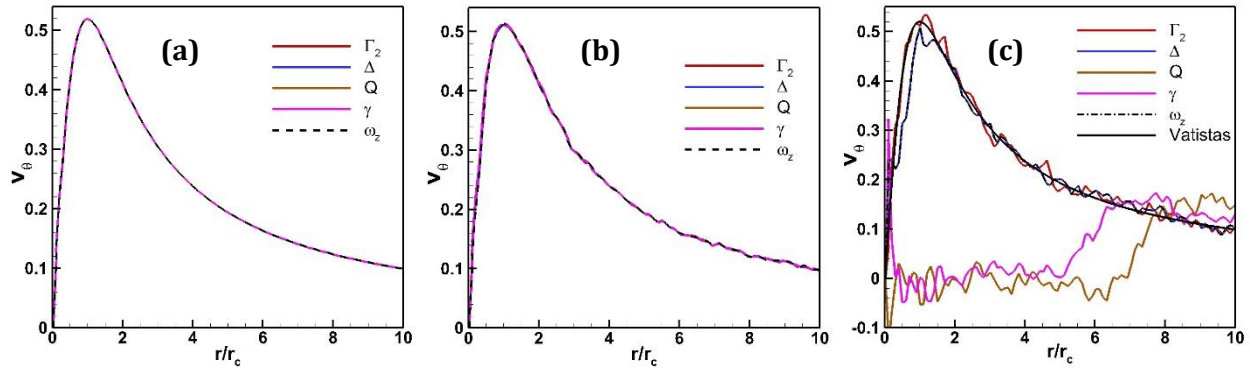


Figure 6: Vatisas Vortex. Swirl velocity vs radial distance with different criteria. Noise 0% (a), noise 20% (b) and noise 90% (c).

## 4.2 Blade Tip Vortex

A typical event that is faced in the case of measurements on rotors, propellers or windmills, is the blade passage in the measurement area (Figure 7-a). This involves the presence of strong laser reflections, which reduce the quality of the measurements and generate a large number of spurious vectors (Figure 7-b) thus invalidating the application of the vortex identification methods based on the velocity gradient. The Q-criterion shows a large number of strong peaks distributed along the path of the rotor blade whereas the tip vortices are depicted by weaker peaks and consequently not validated as shown in Figure 8-a. Analogous behaviour is obtained by  $\Delta$ ,  $\omega_z$  and  $\gamma$  criteria, positioning all the centres on the blade trajectory.

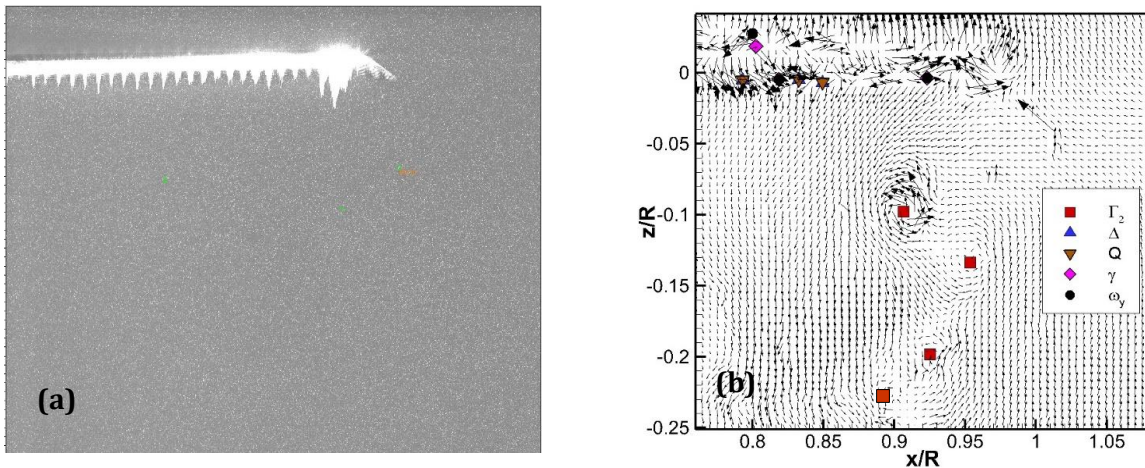


Figure 7: PIV image characterized by rotor blade passage (a) and related velocity field (b)

The  $\Gamma_2$ -criterion also senses the presence of the blade showing a series of peaks which however not reach the threshold value ( $\Gamma_2 < \frac{2}{\pi}$ ). On the contrary, the tip vortices are detected and validated by intense peaks that exceed the threshold value ( $\Gamma_2 > \frac{2}{\pi}$ ) and red coloured in Figure 8-b.

The second test case is selected at a distance of about one radius downstream the rotor disc, a region characterized by high turbulent flow due to the interaction of the blade tip vortices. The Q-criterion identifies correctly the vortical structures in the velocity fields as shown in Figure 9-a, but the peaks of the vortex are exceeded in intensity by spurious peaks that do not allow their identification. The majority of the peaks are located on the lower left side of the flow velocity. The  $\Gamma_2$ -criterion validates three main peaks above the threshold value of  $2 / \pi$  and red coloured in the Figure 9-b, corresponding to the vortices present in the flow field. The identified centres are plotted together with the image velocity field in Figure 10.

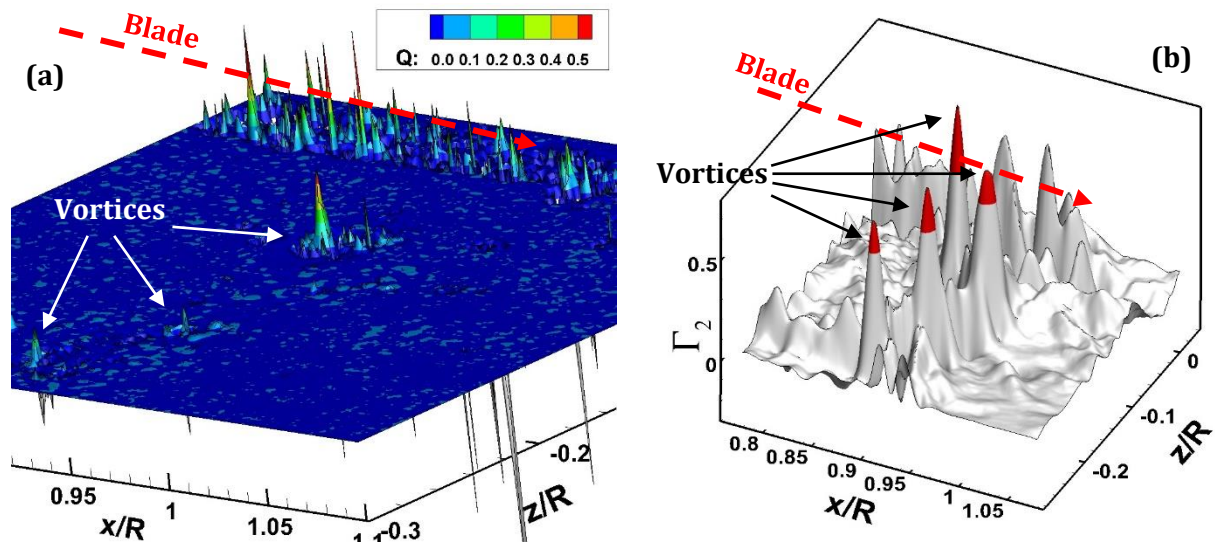


Figure 8: Q-criterion (left) and  $\Gamma_2$ -criterion (right) applied to the velocity field with blade passage.

To conclude, the complete main rotor downwash coloured ensemble average velocity map is shown in Figure 11 (a). The image presents the shear layer region between the inner downwash and the outer still air. The different vortex detection criteria were applied to the full set of instantaneous velocity fields. The position of each blade tip vortex detected by  $\Gamma_2$ , Q and maximum of  $\omega_z$  are shown in Figure 11 (b), (c) and (d) respectively together with the shear layer boundary as reference. The  $\Gamma_2$  criterion shows better characteristics of robustness and reliability than the others do.

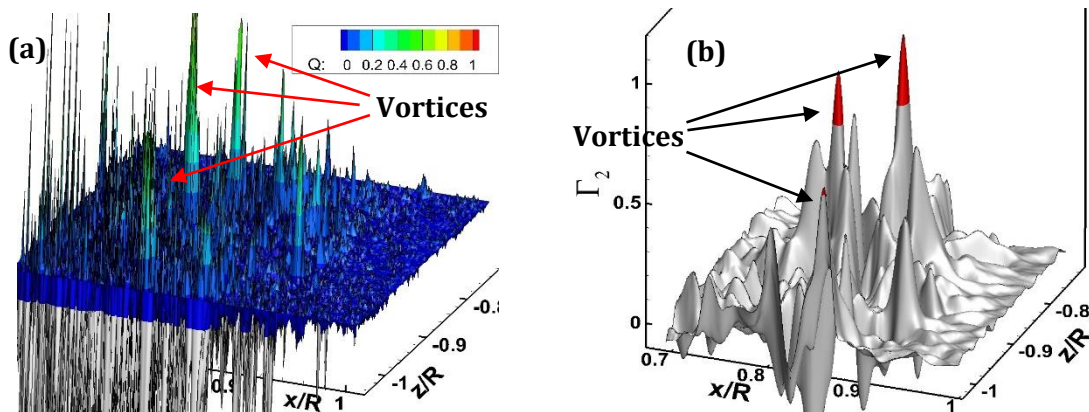


Figure 9: Q-criterion (a) and  $\Gamma_2$ -criterion (b) applied to the turbulent velocity field.

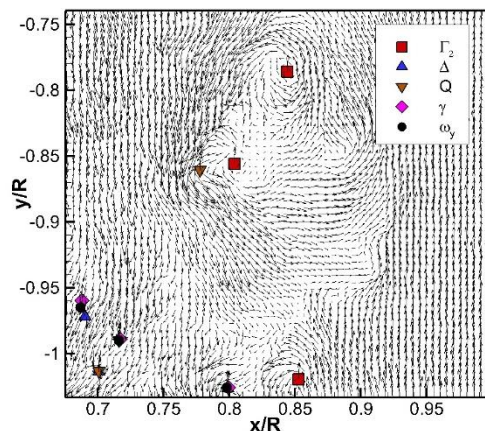


Figure 10: Flow velocity field in the wake turbulent region.

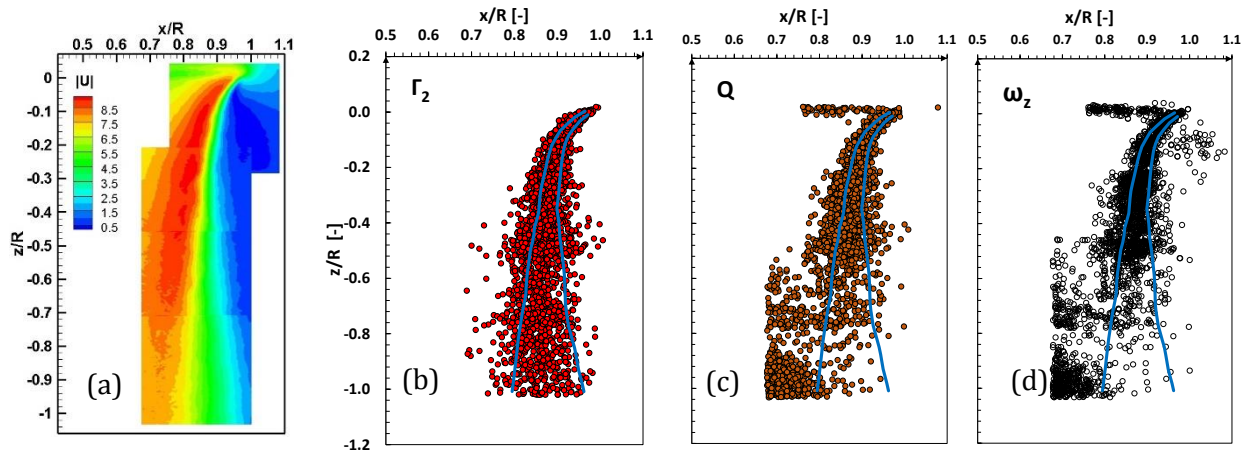


Figure 11: Main rotor downwash velocity (a), blade tip vortices detected by  $\Gamma_2$  (b),  $Q$  (c) and  $\omega_z$  (d).

$\Gamma_2$  is not affected by the blade passage at  $z/R=0$ , the centres are confined in the shear layer boundary with a uniform distribution and do not present the centres concentration on the left bottom corner outside the shear layer region.

## 5 Conclusions

An effective criterion for detecting vortices within PIV data has been investigated. For this purpose, the  $\Gamma_2$  method was selected and compared with some of the most popular vortex identification criteria. The different criteria were tested on special synthetic velocity fields as well as real PIV data. In order to assess the reliability of the  $\Gamma_2$  criterion, a parametric investigation was carried out by using numerically-generated velocity fields containing a single (main) or a couple (main plus secondary) of theoretical vortices, co-rotating or counter rotating. The synthetic velocity fields presented different spatial resolution and noise levels to test the reliability of the vortex detection criteria.

The results showed a successful vortex detection for all the methods for the single vortex without noise, whereas only the  $\Gamma_2$  criterion was able to confine the vortex region and identify the vortex centre with the increase of noise. Furthermore, the parametric study on the single vortex suggested the appropriate value of the domain radius to be used. In case of PIV data, the domain radius should be selected as close as possible to the value of the vortex core radius.

The  $\Gamma_2$  criterion presented remarkable results in terms of robustness and reliability on the real PIV data, in particular for the case of the strong laser reflection in the measurement region. It can be then concluded that this criterion can be a valid alternative to complex algorithm for masking the images removing the laser reflection or to strong data filtering aimed at removing spurious vectors. Furthermore, the  $\Gamma_2$  criterion has shown to be quite robust because the method does not require any fine tuning or the selection of threshold values for an optimization, once the radius has been selected.

## References

- Chakraborty P, Balachandar S and Adrian RJ (2005) On the relationships between local vortex identification schemes. *J. Fluid Mech.*, 535:189–214
- Chong MS (1990) A general classification of three-dimensional flow fields. *Phys. Fluids A2*, 765-777.
- Dallmann U (1983) Topological structures of three-dimensional flow separation. DFVLR-IB Report No. 221-82 A07

13th International Symposium on Particle Image Velocimetry – ISPIV 2019  
Munich, Germany, July 22-24, 2019

De Gregorio F, Visingardi A, Nargi RE (2018) Investigation of a Helicopter Model Rotor Wake interacting with a Cylindrical Sling Load. Proceedings of 44th European Rotorcraft Forum, Delft, The Netherlands, September 18-21

Graftieaux L, Michard M and Grosjean N (2001) Combining PIV, POD and vortex identification algorithms for the study of unsteady turbulent swirling flows. Meas. Sci. Technol. 12:1422–1429

Hunt JCR, Wray AA and Moin P (1988) Eddies, stream, and convergence zones in turbulent flows. Centre for Turbulence Research Report CTR-S88:193–208

Kolar V (2007) Vortex identification: New requirements and limitation. Journal of Heat and Fluid Flow. 28:638-652

Lugt, HJ (1983) Vortex Flow in Nature and Technology. Wiley

Martin PB, Pugliese GJ, Leishman JG, Anderson SL, (2000 ) Stereoscopic PIV measurement in the wake of a hovering rotor. In 56th American Helicopter Society Annual Forum, Virginia Beach, VA, USA, May 2-4

Michard M and Favelier T (2004) Développement d'un critère d'identification de structures tourbillonnaires adapté aux mesures de vitesse par PIV. In 9<sup>o</sup> Congrès Francophone de Vélocimétrie Laser, Bruxelles, September 14-17

Mulleners K and Raffel M (2011) The onset of dynamic stall revisited. Exp Fluids 52:779-793

Robinson SK (1991) Coherent motion in turbulent boundary layer. Annual Review of Fluid Mechanics, 23:601–639

Vatistas GH (1998) New Model for Intense Self-Similar Vortices. Journal of Propulsion and Power, 14:462-469

Visingardi A, De Gregorio F, Schwarz T, Schmid M et al, (2017) Forces on Obstacles in Rotor Wake – A GARTEUR Action Group, in 43rd European Rotorcraft Forum, Milan, Italy, September 12-15

Vollmers H, Kreplin HP, Meier HU (1983) Separation and vertical type flow around a prolate spheroid – Evaluation of relevant parameters. In Proc. of the AGARD Symposium on Aerodynamics of Vortical Type Flows in Three Dimensions, Rotterdam, AGARDCP-342, p14.1-14.14

Vollmers H (2001) Detection of vortices and quantitative evaluation of their main parameters from experimental velocity data. Meas. Sci. Technol. 12:1199-1207